DOI: 10.11650/tjm/230702

Equal Lower-order Finite Elements of Least-squares Type in Biot Poroelasticity Modeling

Hsueh-Chen Lee* and Hyesuk Lee

Abstract. We investigate the behavior of the approximate solution of Biot's consolidation model using a weighted least-squares (WLS) finite element method. The model describes the fluid flow in a deformable porous medium, with variables for fluid pressure, velocity, and displacement. The WLS functional is defined based on the stress-displacement formulation, with the symmetry condition of the stress and the weight that depends on the time step size for the temporal discretization of the model. An a priori error estimate for the first-order linearized least squares (LS) system is analyzed, and its validity is confirmed through numerical results. By using continuous piecewise linear finite element spaces for all variables and adjusting the weight appropriately, we obtain optimal error convergence rates for all variables. Additionally, we present two numerical examples to demonstrate the implementation of the WLS method for benchmark problems.

1. Introduction

Poroelasticity is a model that describes the time-dependent coupling between fluid flow and deformation in an elastic porous material, which often involves data with high uncertainty. For some applications, studies have shown that using equal lower-order elements is more accurate than using higher-order elements [9]. Moreover, this approach is easier to implement in large simulation codes as it results in less dense matrices on supercomputers [3,8]. While the linear equal-order finite element approach offers several computational advantages, the Galerkin finite element method can lead to instabilities due to space incompatibility. To address this issue, the least-squares (LS) finite element method can be used, which does not require the *inf-sup* condition [3,13].

There have been several reports on LS methods to simulate the four-field Biot model [11, 12, 15, 17]. In [17], Tchonkova et al. presented a mixed least-squares method with

Received April 9, 2023; Accepted July 5, 2023.

Communicated by Jenn-Nan Wang.

2020 Mathematics Subject Classification. 65N30.

Key words and phrases. least-squares method, time dependent weight, Cantilever bracket problem, Biot poroelasticity model.

The first author is grateful for the Taiwan NSTC grant 111-2115-M-160-003 and the second author is grateful for the NSF under grant number DMS-2207971.

*Corresponding author.

equal order linear interpolation function to minimize the combined LS functional of the flow and elasticity parts. In addition, they demonstrated that equal-order interpolation in a cantilever beam problem did not exhibit any numerical instability, such as shear locking or oscillations. In [11,12], the standard least-squares functional was formulated as the sum of the residuals of equations measured in the L^2 -norm, based on H^{div} -conforming Raviart—Thomas spaces for the velocity and stress components. In [15], time-dependent weights and a scaled stress-displacement equation were used in the L^2 least-squares functional to simulate the intracranial brain pressure. Cai and Starke [5] showed that the scaled stress-displacement equation was permissible for the piecewise linear finite element spaces.

In [11, 15], WLS methods for poroelasticity were introduced and analyzed for finite element error estimates. In those studies, WLS functionals were defined based on the stress-displacement formulation, and the weight depends on Δt , the time step size chosen for the temporal discretization. This work aims to extend the investigation of the WLS method, introduced in [15], by testing it numerically using linear equal-order basis functions for all variables and different weights. Furthermore, we propose an a posteriori error estimator [14] for the WLS method to verify its convergence rate in a non-physical problem with a known solution. We then use this estimator as a mesh refinement criterion to refine the grid points and compare the numerical results for a physical problem.

We also extend the implementation to simulate the cantilever bracket problem considered in [16,18]. In [18], the mixed finite element method utilizes continuous bilinear elements for displacement and the lowest-order Raviart—Thomas space for flow variables. In contrast, we use linear equal-order finite elements to solve the Biot model. It is important to note that equal-order linear elements do not satisfy compatibility conditions between finite element spaces and offer advantages in terms of ease of implementation. Despite this difference, our approach results are comparable to the mixed finite element method presented in [18].

The rest of this paper is organized as follows. Section 2 presents the model equations. Section 3 introduces the WLS functional with the scaled stress-displacement equation and the analysis for the functional. Section 4 presents finite element spaces and an error estimate of the finite element solution. Section 5 provides two numerical examples, where numerical solutions by different sets of weights and stress equations are compared, and finally, conclusions follow in Section 6.

2. Model equations

Biot's consolidation model provides a general description of the mechanical behavior of poroelastic materials. Biot's poroelasticity model is composed of the fluid mass balance in the pores of the matrix, Darcy law, and the momentum equation for the balance of total

forces [1,2]. Let Ω be a bounded, connected domain in \mathbb{R}^d , d=2,3 with the Lipschitz boundary $\partial\Omega$. The governing equations are as follows:

(2.1)
$$\nabla \cdot \mathbf{u} + \frac{\partial}{\partial t} (c_s p + \alpha \nabla \cdot \boldsymbol{\eta}) = f_s \quad \text{in } \Omega,$$

(2.2)
$$\mathbf{u} + K\nabla p = \mathbf{0} \quad \text{in } \Omega,$$

(2.3)
$$-2\mu\nabla\cdot\boldsymbol{\epsilon}(\boldsymbol{\eta}) - \lambda\nabla(\nabla\cdot\boldsymbol{\eta}) + \alpha\nabla p = \mathbf{f}_b \quad \text{in } \Omega,$$

where \mathbf{u} denotes the fluid velocity, $\boldsymbol{\eta}$ denotes the displacement field, p is the pore pressure of the fluid and $\boldsymbol{\epsilon}(\boldsymbol{\eta}) := 0.5(\nabla \boldsymbol{\eta} + \nabla \boldsymbol{\eta}^T)$ is the standard strain rate tensor. The parameter c_s is the constrained specific storage coefficient, α is the Biot–Willis coefficient, and $K = \kappa/\mu_f$ is the hydraulic conductivity with κ being the permeability and μ_f being the fluid viscosity. In (2.3) μ and λ are the Lamé coefficients, which is computed by the Young's modulus E and the Poisson ratio ν :

$$\mu = \frac{E\nu}{2(1+\nu)}, \quad \lambda = \frac{E\nu}{(1+\nu)(1-2\nu)}.$$

The right-hand side functions f_s , \mathbf{f}_b are the source/sink term and the body force, respectively. Let the boundary of domain, $\partial\Omega$ be decomposed into two pairs of disjoint sets such that $\partial\Omega = \Gamma_{pD} \cup \Gamma_{pN}$ and $\partial\Omega = \Gamma_{dD} \cup \Gamma_{dN}$ with the Neumann and Dirichlet boundaries. The Biot model is completed with the boundary conditions

$$p = 0$$
 on Γ_{pD} , $\mathbf{u} \cdot \mathbf{n} = 0$ on Γ_{pN} , $\eta = \mathbf{0}$ on Γ_{dD} , $\sigma \cdot \mathbf{n} = \mathbf{0}$ on Γ_{dN} ,

where \mathbf{n} is an outward unit normal vector and we consider homogeneous boundary conditions for simplicity. We also have the following initial conditions

$$p = p_0$$
, $\boldsymbol{\eta} = \boldsymbol{\eta}_0$ for $t = 0$.

In order to formulate the least squares functional, we introduce the elastic stiffness tensor \mathcal{C} [6]:

(2.4)
$$C\epsilon(\eta) = 2\mu\epsilon(\eta) + \lambda(\operatorname{tr}\epsilon(\eta))\mathbf{I},$$

which can be regarded as a symmetric positive linear mapping. However, C is the linearity of the elastic stiffness tensor, where it is assumed to be linear. Let σ be the stress tensor from linear elasticity satisfying

(2.5)
$$\boldsymbol{\sigma} = \mathcal{C}\boldsymbol{\epsilon}(\boldsymbol{\eta}).$$

In finite element approximations of the linear elasticity with a large $\lambda > 0$ for nearly incompressible materials, the equation

$$C^{-1} \sigma = \epsilon(\eta)$$

is usually considered instead of (2.9) for a locking-free formulation, where C^{-1} is the fourth-order compliance tensor given by

$$C^{-1}\boldsymbol{\sigma} = \frac{1}{2\mu}\boldsymbol{\sigma} - \frac{\lambda}{2\mu(d\lambda + 2\mu)}(\operatorname{tr}\boldsymbol{\sigma})\mathbf{I},$$

where d is the dimension of Ω .

Using the backward Euler method for the time derivative and the additional stress variable defined in (2.5), the temporal discretized first order system for (2.1)–(2.3) can be written as

$$\mathcal{L}\mathbf{U} = \mathbf{F} \quad \text{in } \Omega,$$

where $\mathcal{L} := (\mathcal{L}_1, \mathcal{L}_2, \mathcal{L}_3, \mathcal{L}_4)$ and $\mathbf{F} := (\mathbf{f}_1, \mathbf{f}_2, \mathbf{f}_3, \mathbf{f}_4) = (f_s + \frac{1}{\Delta t}(\alpha \nabla \cdot \boldsymbol{\eta}^{\text{old}} + c_s p^{\text{old}}), \mathbf{0}, \mathbf{f}_b, \mathbf{0}),$ in which

(2.6)
$$\mathcal{L}_1 \mathbf{U} := \nabla \cdot \mathbf{u} + \frac{1}{\Delta t} (c_s p + \alpha \nabla \cdot \boldsymbol{\eta}),$$

(2.7)
$$\mathcal{L}_2 \mathbf{U} := \mathbf{u} + K \nabla p,$$

(2.8)
$$\mathcal{L}_3 \mathbf{U} := -\nabla \cdot (\boldsymbol{\sigma} - \alpha p \mathbf{I}),$$

(2.9)
$$\mathcal{L}_4 \mathbf{U} := \boldsymbol{\sigma} - \mathcal{C} \boldsymbol{\epsilon}(\boldsymbol{\eta}),$$

where Δt is a fixed time step size and p^{old} , η^{old} denote the pressure and displacement fields at the previous time-step, respectively.

3. Least squares functional

Let $H^s(\Omega)$, $s \geq 0$, be the Sobolev spaces with the standard associated inner products $(\cdot,\cdot)_s$ and their respective norms $\|\cdot\|_s$. For s=0, $H^s(\Omega)$ coincides with $L^2(\Omega)$, and $\|\cdot\|$ is used for $\|\cdot\|_0$. In order to consider the least squares functional, we first introduce the functional spaces for $(\sigma, \eta, \mathbf{u}, p)$:

$$\mathbf{S} := \{ \boldsymbol{\tau} \in \mathbf{H}_{div}(\Omega) : \tau_{ij} = \tau_{ji}, 1 \leq i, j \leq d, \boldsymbol{\tau} \cdot \mathbf{n} = \mathbf{0} \text{ on } \Gamma_{dN} \},$$

$$\boldsymbol{\Sigma} := \{ \boldsymbol{\xi} \in \mathbf{H}^{1}(\Omega) : \boldsymbol{\xi} = \mathbf{0} \text{ on } \Gamma_{dD} \},$$

$$\mathbf{X} := \{ \mathbf{u} \in \mathbf{H}_{div}(\Omega) : \mathbf{u} \cdot \mathbf{n} = 0 \text{ on } \Gamma_{pN} \},$$

$$Q := \{ q \in H^{1}(\Omega) : q = 0 \text{ on } \Gamma_{pD} \}$$

and define the product space $\Phi = \mathbf{S} \times \mathbf{\Sigma} \times \mathbf{X} \times Q$. The standard WLS functional for (2.6)–(2.9) is given by

(3.1)
$$\mathcal{J}_s(\boldsymbol{\sigma}, \boldsymbol{\eta}, \mathbf{u}, p; \mathbf{F}) := \sum_{j=1}^4 W_j \|\mathcal{L}_j \mathbf{U} - \mathbf{f}_j\|^2,$$

where W_j for j = 1, 2, 3, 4 are positive constants.

In this work, we consider a scaled stress equation instead of (2.9) for the proper balance of terms in the WLS functional to be introduced. First, we derive the fractional operator $C^{1/2}\epsilon(\eta)$ satisfying

(3.2)
$$\|\mathcal{C}^{1/2}\boldsymbol{\epsilon}(\boldsymbol{\eta})\|^2 = (\mathcal{C}\boldsymbol{\epsilon}(\boldsymbol{\eta}), \boldsymbol{\epsilon}(\boldsymbol{\eta})).$$

With the definition of \mathcal{C} , (2.4),

(3.3)
$$(\mathcal{C}\boldsymbol{\epsilon}(\boldsymbol{\eta}), \boldsymbol{\epsilon}(\boldsymbol{\eta})) = 2\mu \|\boldsymbol{\epsilon}(\boldsymbol{\eta})\|^2 + \lambda((\operatorname{tr}\boldsymbol{\epsilon}(\boldsymbol{\eta}))\mathbf{I}, \boldsymbol{\epsilon}(\boldsymbol{\eta}))$$
$$= 2\mu \|\boldsymbol{\epsilon}(\boldsymbol{\eta})\|^2 + \lambda(\operatorname{tr}\boldsymbol{\epsilon}(\boldsymbol{\eta}), \operatorname{tr}\boldsymbol{\epsilon}(\boldsymbol{\eta}))$$
$$= 2\mu \|\boldsymbol{\epsilon}(\boldsymbol{\eta})\|^2 + \lambda \|\operatorname{tr}\boldsymbol{\epsilon}(\boldsymbol{\eta})\|^2.$$

In order to have (3.2) and (3.3) satisfied, $C^{1/2}\epsilon$ should be in the form of

(3.4)
$$C^{1/2} \epsilon(\boldsymbol{\eta}) = \sqrt{2\mu} \epsilon(\boldsymbol{\eta}) + X(\operatorname{tr} \epsilon(\boldsymbol{\eta})) \mathbf{I}$$

for some scalar X to be determined. Using (3.4)

(3.5)

$$\|\mathcal{C}^{1/2}\boldsymbol{\epsilon}(\boldsymbol{\eta})\|^{2} = (\mathcal{C}^{1/2}\boldsymbol{\epsilon}(\boldsymbol{\eta}), \mathcal{C}^{1/2}\boldsymbol{\epsilon}(\boldsymbol{\eta}))$$

$$= 2\mu\|\boldsymbol{\epsilon}(\boldsymbol{\eta})\|^{2} + X^{2}((\operatorname{tr}\boldsymbol{\epsilon}(\boldsymbol{\eta}))\mathbf{I}, (\operatorname{tr}\boldsymbol{\epsilon}(\boldsymbol{\eta}))\mathbf{I}) + 2\sqrt{2\mu}X((\operatorname{tr}\boldsymbol{\epsilon}(\boldsymbol{\eta}))\mathbf{I}, (\operatorname{tr}\boldsymbol{\epsilon}(\boldsymbol{\eta}))\mathbf{I})$$

$$= 2\mu\|\boldsymbol{\epsilon}(\boldsymbol{\eta})\|^{2} + dX^{2}\|\operatorname{tr}\boldsymbol{\epsilon}(\boldsymbol{\eta})\|^{2} + 2\sqrt{2\mu}X\|\operatorname{tr}\boldsymbol{\epsilon}(\boldsymbol{\eta})\|^{2}.$$

Note that $\epsilon(\eta)$: $\mathbf{I} = \operatorname{tr} \epsilon(\eta)$. Then (3.2), (3.3) and (3.5) imply

$$2\mu \|\boldsymbol{\epsilon}(\boldsymbol{\eta})\|^2 + \lambda \|\operatorname{tr}\boldsymbol{\epsilon}(\boldsymbol{\eta})\|^2 = 2\mu \|\boldsymbol{\epsilon}(\boldsymbol{\eta})\|^2 + dX^2 \|\operatorname{tr}\boldsymbol{\epsilon}(\boldsymbol{\eta})\|^2 + 2\sqrt{2\mu}X \|\operatorname{tr}\boldsymbol{\epsilon}(\boldsymbol{\eta})\|^2,$$

i.e.,

$$dX^2 + 2\sqrt{2\mu}X - \lambda = 0.$$

Solving the quadratic equation, we have $X = \frac{-\sqrt{2\mu} \pm \sqrt{2\mu + d\lambda}}{d}$. Taking "+" sign here as both parameters in \mathcal{C} are positive, we obtain

(3.6)
$$C^{1/2} \epsilon(\boldsymbol{\eta}) = \sqrt{2\mu} \epsilon(\boldsymbol{\eta}) + \frac{-\sqrt{2\mu} + \sqrt{2\mu + d\lambda}}{d} (\operatorname{tr} \epsilon(\boldsymbol{\eta})) \mathbf{I}.$$

The inverse fractional operator $C^{-1/2}$ can be derived similarly. Consider

(3.7)
$$\|\mathcal{C}^{-1/2}\boldsymbol{\sigma}\|^2 = (\mathcal{C}^{-1}\boldsymbol{\sigma},\boldsymbol{\sigma}),$$

where the inverse operator C^{-1} is defined as (see (2.4) in [4])

$$C^{-1}\boldsymbol{\sigma} = \frac{1}{2\mu}\boldsymbol{\sigma} - \frac{\lambda}{2\mu(d\lambda + 2\mu)}(\operatorname{tr}\boldsymbol{\sigma})\mathbf{I}.$$

By the definition of C^{-1} ,

(3.8)
$$(\mathcal{C}^{-1}\boldsymbol{\sigma},\boldsymbol{\sigma}) = \frac{1}{2\mu} \|\boldsymbol{\sigma}\|^2 - \frac{\lambda}{2\mu(d\lambda + 2\mu)} \|\operatorname{tr}\boldsymbol{\sigma}\|^2.$$

In order to have (3.7) satisfied, $C^{-1/2}\sigma$ should be in the form of

(3.9)
$$C^{-1/2}\boldsymbol{\sigma} = \frac{1}{\sqrt{2\mu}}\boldsymbol{\sigma} + X(\operatorname{tr}\boldsymbol{\sigma})\mathbf{I}$$

for some scalar X to be determined. Using (3.9),

(3.10)
$$\|\mathcal{C}^{-1/2}\boldsymbol{\sigma}\|^2 = (\mathcal{C}^{-1/2}\boldsymbol{\sigma}, \mathcal{C}^{-1/2}\boldsymbol{\sigma})$$

$$= \frac{1}{2\mu} \|\boldsymbol{\sigma}\|^2 + dX^2 \|\operatorname{tr}\boldsymbol{\sigma}\|^2 + \frac{2}{\sqrt{2\mu}} X \|\operatorname{tr}\boldsymbol{\sigma}\|^2.$$

Now (3.7), (3.8) and (3.10) imply

$$\frac{1}{2\mu} \|\boldsymbol{\sigma}\|^2 - \frac{\lambda}{2\mu(d\lambda + 2\mu)} \|\operatorname{tr}\boldsymbol{\sigma}\|^2 = \frac{1}{2\mu} \|\boldsymbol{\sigma}\|^2 + dX^2 \|\operatorname{tr}\boldsymbol{\sigma}\|^2 + \frac{2}{\sqrt{2\mu}} X \|\operatorname{tr}\boldsymbol{\sigma}\|^2,$$

i.e.,

$$dX^2 + \frac{2}{\sqrt{2\mu}}X + \frac{\lambda}{2\mu(d\lambda + 2\mu)} = 0.$$

Solving the quadratic equation, we have $X = \frac{1}{d} \left(-\frac{1}{\sqrt{2\mu}} \pm \frac{1}{\sqrt{d\lambda + 2\mu}} \right)$, and therefore,

(3.11)
$$C^{-1/2}\boldsymbol{\sigma} = \frac{1}{\sqrt{2\mu}}\boldsymbol{\sigma} + \frac{1}{d}\left(-\frac{1}{\sqrt{2\mu}} + \frac{1}{\sqrt{d\lambda + 2\mu}}\right)(\operatorname{tr}\boldsymbol{\sigma})\mathbf{I}.$$

Being scaled by $C^{-1/2}$, (2.9) can be written in the following alternate formulation [4, 5, 11]:

(3.12)
$$\mathcal{C}^{-1/2}\boldsymbol{\sigma} - \mathcal{C}^{1/2}\boldsymbol{\epsilon}(\boldsymbol{\eta}) = \mathbf{0},$$

where $C^{1/2}\epsilon(\eta)$ and $C^{-1/2}\sigma$ are given by (3.6) and (3.11), respectively.

We now define the WLS functionals with positive constants W_j for (2.6)–(2.8) and (3.12):

(3.13)
$$\mathcal{J}(\boldsymbol{\sigma}, \boldsymbol{\eta}, \mathbf{u}, p; \mathbf{F}) := \sum_{j=1}^{3} W_j \|\mathcal{L}_j \mathbf{U} - \mathbf{f}_j\|^2 + W_4 \|\mathcal{L}_5 \mathbf{U} - \mathbf{f}_4\|^2,$$

in which $\mathcal{L}_5\mathbf{U} := \mathcal{C}^{-1/2}\boldsymbol{\sigma} - \mathcal{C}^{1/2}\boldsymbol{\epsilon}(\boldsymbol{\eta})$. The least-squares problem for the first order system (2.6)–(2.8) and (3.12) is to minimize the quadratic functional $\mathcal{J}(\boldsymbol{\sigma}, \boldsymbol{\eta}, \mathbf{u}, p; \mathbf{F})$ over $\boldsymbol{\Phi}$, that is, find $(\boldsymbol{\sigma}, \boldsymbol{\eta}, \mathbf{u}, p) \in \boldsymbol{\Phi}$ such that

(3.14)
$$\mathcal{J}(\boldsymbol{\sigma}, \boldsymbol{\eta}, \mathbf{u}, p; \mathbf{F}) = \inf_{(\boldsymbol{\tau}, \boldsymbol{\xi}, \mathbf{v}, q) \in \boldsymbol{\Phi}} \mathcal{J}(\boldsymbol{\tau}, \boldsymbol{\xi}, \mathbf{v}, q; \mathbf{F}).$$

For (3.13) we consider the WLS functional with the weights $(W_1, W_2, W_3, W_4) = (\Delta t^2, 1, \Delta t, 1)$:

(3.15)
$$\mathcal{J}_{\Delta t^2}(\boldsymbol{\sigma}, \boldsymbol{\eta}, \mathbf{u}, p; \mathbf{F}) := \Delta t^2 \|\mathcal{L}_1 \mathbf{U} - \mathbf{f}_1\|^2 + \|\mathcal{L}_2 \mathbf{U} - \mathbf{f}_2\|^2 + \Delta t \|\mathcal{L}_3 \mathbf{U} - \mathbf{f}_3\|^2 + \|\mathcal{L}_5 \mathbf{U} - \mathbf{f}_4\|^2.$$

Define the scaled norm

$$\|(\boldsymbol{\tau}, \boldsymbol{\xi}, \mathbf{v}, q)\|_{\Delta t}^{2} = \|\nabla \cdot \boldsymbol{\tau}\|^{2} + \|\mathcal{C}^{-1/2}\boldsymbol{\tau}\|^{2} + \|\mathcal{C}^{1/2}\boldsymbol{\epsilon}(\boldsymbol{\xi})\|^{2} + (\Delta t)^{2}\|\nabla \cdot \mathbf{v}\|^{2} + \Delta t\|\mathbf{v}\|^{2} + \Delta t\|\nabla q\|^{2} + \|q\|^{2}$$

for all $(\tau, \xi, \mathbf{v}, q) \in \Phi$. In [15], we used the $(W_1, W_2, W_3, W_4) = (\Delta t, 1, \Delta t, 1)$ for \mathcal{J} in (3.13), i.e.,

(3.16)
$$\mathcal{J}_{\Delta t}(\boldsymbol{\sigma}, \boldsymbol{\eta}, \mathbf{u}, p; \mathbf{F}) := \Delta t \|\mathcal{L}_1 \mathbf{U} - \mathbf{f}_1\|^2 + \|\mathcal{L}_2 \mathbf{U} - \mathbf{f}_2\|^2 + \Delta t \|\mathcal{L}_3 \mathbf{U} - \mathbf{f}_3\|^2 + \|\mathcal{L}_5 \mathbf{U} - \mathbf{f}_4\|^2.$$

and established the following a priori error estimate: $\forall (\tau, \xi, \mathbf{v}, q) \in \Phi$,

$$(3.17) \overline{C}_1 \| (\boldsymbol{\tau}, \boldsymbol{\xi}, \mathbf{v}, q) \|_{\Delta t}^2 \le \mathcal{J}_{\Delta t} (\boldsymbol{\tau}, \boldsymbol{\xi}, \mathbf{v}, q; \mathbf{0}) \le \overline{C}_2 \| (\boldsymbol{\tau}, \boldsymbol{\xi}, \mathbf{v}, q) \|_{\Delta t}^2$$

for a fixed $\Delta t \leq 1$ and positive constants \overline{C}_1 , \overline{C}_2 dependent on Δt .

Using (3.17), we now derive the coercivity and continuity estimates of the functional $\mathcal{J}_{\Delta t^2}$ in the following theorem.

Theorem 3.1. There are positive constants \overline{C} , \overline{C}_2 dependent on Δt satisfying

$$\overline{C}\|(\boldsymbol{\tau}, \boldsymbol{\xi}, \mathbf{v}, q)\|_{\Delta t}^2 \leq \mathcal{J}_{\Delta t^2}(\boldsymbol{\tau}, \boldsymbol{\xi}, \mathbf{v}, q; \mathbf{0}) \leq \overline{C}_2\|(\boldsymbol{\tau}, \boldsymbol{\xi}, \mathbf{v}, q)\|_{\Delta t}^2$$

for all $(\tau, \xi, \mathbf{v}, q) \in \Phi$.

Proof. For the fixed $\Delta t \leq 1$, $\Delta t \mathcal{J}_{\Delta t}(\boldsymbol{\sigma}, \boldsymbol{\eta}, \mathbf{u}, p; \mathbf{F}) \leq \mathcal{J}_{\Delta t^2}(\boldsymbol{\sigma}, \boldsymbol{\eta}, \mathbf{u}, p; \mathbf{F})$. We have the following result using (3.17),

$$\Delta t \overline{C}_1 \| (\boldsymbol{\tau}, \boldsymbol{\xi}, \mathbf{v}, q) \|_{\Delta t}^2 \le \Delta t \mathcal{J}_{\Delta t}(\boldsymbol{\sigma}, \boldsymbol{\eta}, \mathbf{u}, p; \mathbf{F}) \le \mathcal{J}_{\Delta t^2}(\boldsymbol{\sigma}, \boldsymbol{\eta}, \mathbf{u}, p; \mathbf{F}).$$

Let the constant $\overline{C} = \Delta t \overline{C}_1$,

$$\overline{C}\|(\boldsymbol{\tau},\boldsymbol{\xi},\mathbf{v},q)\|_{\Delta t}^2 \leq \mathcal{J}_{\Delta t^2}(\boldsymbol{\sigma},\boldsymbol{\eta},\mathbf{u},p;\mathbf{F}) \leq \mathcal{J}_{\Delta t}(\boldsymbol{\sigma},\boldsymbol{\eta},\mathbf{u},p;\mathbf{F}) \leq \overline{C}_2\|(\boldsymbol{\tau},\boldsymbol{\xi},\mathbf{v},q)\|_{\Delta t}^2$$

for all
$$(\boldsymbol{\tau}, \boldsymbol{\xi}, \mathbf{v}, q) \in \boldsymbol{\Phi}$$
.

4. Finite element approximation

For the finite element approximation of (2.1)–(2.3), we assume that the domain Ω is a polygon and that \mathcal{T}_h is a collection of finite elements such that $\Omega = \bigcup_{T \in \mathcal{T}_h} T$ with $h = \max\{\operatorname{diam}(T) : T \in \mathcal{T}_h\}$. Assume that the triangulation \mathcal{T}_h is shape-regular and satisfies the assumption for inverse estimates [13]. The grid size is defined as $h = 2\sqrt{|\Omega|}/\sqrt{N}$, where $|\Omega|$ is the area of the domain and N is the number of elements in \mathcal{T}_h . Define finite element spaces for the approximate of $(\sigma, \eta, \mathbf{u}, p)$:

$$\mathbf{S}^{h} = \{ \boldsymbol{\tau}^{h} : \boldsymbol{\tau}^{h} \in \mathbf{X} \cap C^{0}(\Omega)^{2 \times 2}, \mathbf{v}^{h}|_{T} \in P_{r}(T)^{2 \times 2}, \forall T \in \mathcal{T}_{h} \},$$

$$\boldsymbol{\Sigma}^{h} = \{ \boldsymbol{\xi}^{h} : \boldsymbol{\xi}^{h} \in \boldsymbol{\Sigma} \cap C^{0}(\Omega)^{2}, \boldsymbol{\eta}^{h}|_{T} \in P_{r}(T)^{2}, \forall T \in \mathcal{T}_{h} \},$$

$$\mathbf{X}^{h} = \{ \mathbf{v}^{h} : \mathbf{v}^{h} \in \mathbf{X} \cap C^{0}(\Omega)^{2}, \mathbf{v}^{h}|_{T} \in P_{r}(T)^{2}, \forall T \in \mathcal{T}_{h} \},$$

$$Q^{h} = \{ q^{h} : q^{h} \in Q \cap C^{0}(\Omega), q^{h}|_{T} \in P_{r}(T), \forall T \in \mathcal{T}_{h} \},$$

where P_r denote the piecewise polynomial space of order r, respectively.

We assume the following standard approximation properties:

for $m \leq r$ and l = 0, 1. Then, the discrete least-squares problem for the Biot model is to choose $\Phi^h := \mathbf{S}^h \times \mathbf{\Sigma}^h \times \mathbf{X}^h \times Q^h$ be the finite element subspace of Φ and consider the discrete least-squares problem for the Biot model: compute $(\boldsymbol{\sigma}^h, \boldsymbol{\eta}^h, \mathbf{u}^h, p^h) \in \Phi^h$ such that

(4.2)
$$\mathcal{J}_{\Delta t^{i}}(\boldsymbol{\sigma}^{h}, \boldsymbol{\eta}^{h}, \mathbf{u}^{h}, p^{h}; \mathbf{F}) = \inf_{(\boldsymbol{\tau}^{h}, \boldsymbol{\xi}^{h}, \mathbf{v}^{h}, q^{h}) \in \boldsymbol{\Phi}^{h}} \mathcal{J}_{\Delta t^{i}}(\boldsymbol{\tau}^{h}, \boldsymbol{\xi}^{h}, \mathbf{v}^{h}, q^{h}; \mathbf{F})$$

for i = 1 or 2.

Theorem 4.1. Consider approximating the solution to (2.1)–(2.3) with the condition (4.1). Assume that $(\boldsymbol{\sigma}, \boldsymbol{\eta}, \mathbf{u}, p) \in \boldsymbol{\Phi} \cap H^{m+1}(\Omega)^{2\times 2} \times H^{m+1}(\Omega)^2 \times H^{m+1}(\Omega)^2 \times H^{m+1}(\Omega)$ is the solution to (3.14) and $(\boldsymbol{\sigma}^h, \boldsymbol{\eta}^h, \mathbf{u}^h, p^h) \in \boldsymbol{\Phi}^h$ is the unique approximation solution to (4.2). Then there is a positive constant C which is independent of h such that

(4.3)
$$\mathcal{J}_{\Delta t^{i}}^{1/2}(\boldsymbol{\sigma}^{h}, \boldsymbol{\eta}^{h}, \mathbf{u}^{h}, p^{h}; \mathbf{F}) \leq Ch^{m} (\|\nabla \cdot \boldsymbol{\sigma}\|_{m} + \|\boldsymbol{\sigma}\|_{m} + \|\boldsymbol{\eta}\|_{m+1} + \|\nabla \cdot \mathbf{u}\|_{m} + \|\mathbf{u}\|_{m} + \|p\|_{m+1}),$$

$$(4.4) \qquad \|\boldsymbol{\sigma} - \boldsymbol{\sigma}^h\|_{H_{div}(\Omega)} + \|\nabla(\boldsymbol{\eta} - \boldsymbol{\eta}^h)\| + \|\mathbf{u} - \mathbf{u}^h\|_{H_{div}(\Omega)} + \|\nabla(p - p^h)\|$$

$$\leq Ch^m (\|\nabla \cdot \boldsymbol{\sigma}\|_m + \|\boldsymbol{\sigma}\|_m + \|\boldsymbol{\eta}\|_{m+1} + \|\nabla \cdot \mathbf{u}\|_m + \|\mathbf{u}\|_m + \|p\|_{m+1}),$$

and

(4.5)
$$\|\boldsymbol{\sigma} - \boldsymbol{\sigma}^h\| + \|p - p^h\| + \|\mathbf{u} - \mathbf{u}^h\| + \|\boldsymbol{\eta} - \boldsymbol{\eta}^h\|$$

$$\leq Ch^m (\|\nabla \cdot \boldsymbol{\sigma}\|_m + \|\boldsymbol{\sigma}\|_m + \|\boldsymbol{\eta}\|_{m+1} + \|\nabla \cdot \mathbf{u}\|_m + \|\mathbf{u}\|_m + \|p\|_{m+1})$$

for i = 1 or 2.

Proof. By Theorem 3.1, (3.17), and the approximation properties in (4.1), there exists C > 0 depends on Δt such that

$$\mathcal{J}_{\Delta t^{i}}^{1/2}(\boldsymbol{\sigma}^{h}, \boldsymbol{\eta}^{h}, \mathbf{u}^{h}, p^{h}; \mathbf{F})
= \mathcal{J}_{\Delta t^{i}}^{1/2}(\boldsymbol{\sigma} - \boldsymbol{\sigma}^{h}, \boldsymbol{\eta} - \boldsymbol{\eta}^{h}, \mathbf{u} - \mathbf{u}^{h}, p - p^{h}; \mathbf{0})
\leq C \|(\boldsymbol{\sigma} - \boldsymbol{\sigma}^{h}, \boldsymbol{\eta} - \boldsymbol{\eta}^{h}, \mathbf{u} - \mathbf{u}^{h}, p - p^{h}; \mathbf{0})\|_{\Delta t^{i}}^{1/2}
\leq C h^{m} (\|\nabla \cdot \boldsymbol{\sigma}\|_{m} + \|\boldsymbol{\sigma}\|_{m} + \|\boldsymbol{\eta}\|_{m+1} + \|\nabla \cdot \mathbf{u}\|_{m} + \|\mathbf{u}\|_{m} + \|p\|_{m+1})$$

and

$$\|\boldsymbol{\sigma} - \boldsymbol{\sigma}^h\|_{H_{div}(\Omega)} + \|\nabla(\boldsymbol{\eta} - \boldsymbol{\eta}^h)\| + \|\mathbf{u} - \mathbf{u}^h\|_{H_{div}(\Omega)} + \|\nabla(p - p^h)\|$$

$$\leq \mathcal{J}_{\Delta t^i}^{1/2}(\boldsymbol{\sigma} - \boldsymbol{\sigma}^h, \boldsymbol{\eta} - \boldsymbol{\eta}^h, \mathbf{u} - \mathbf{u}^h, p - p^h; \mathbf{0})$$

$$\leq Ch^m(\|\nabla \cdot \boldsymbol{\sigma}\|_m + \|\boldsymbol{\sigma}\|_m + \|\boldsymbol{\eta}\|_{m+1} + \|\nabla \cdot \mathbf{u}\|_m + \|\mathbf{u}\|_m + \|p\|_{m+1})$$

for i = 1 or 2. Then by the Poincaré inequality and (4.4), we can have that

$$\|\mathbf{u} - \mathbf{u}^h\| \le Ch^m (\|\nabla \cdot \boldsymbol{\sigma}\|_m + \|\boldsymbol{\sigma}\|_m + \|\boldsymbol{\eta}\|_{m+1} + \|\nabla \cdot \mathbf{u}\|_m + \|\mathbf{u}\|_m + \|p\|_{m+1}),$$

$$\|\boldsymbol{\eta} - \boldsymbol{\eta}^h\| \le \|\nabla(\boldsymbol{\eta} - \boldsymbol{\eta}^h)\|$$

$$\le Ch^m (\|\nabla \cdot \boldsymbol{\sigma}\|_m + \|\boldsymbol{\sigma}\|_m + \|\boldsymbol{\eta}\|_{m+1} + \|\nabla \cdot \mathbf{u}\|_m + \|\mathbf{u}\|_m + \|p\|_{m+1}).$$

By the same approach, we can obtain the desired estimates for $||p - p^h||$ and $||\sigma - \sigma^h||$, respectively.

Remark 4.2. The error bounds predicted based on (4.5) are only O(h) in the L^2 -norm for σ , p, \mathbf{u} , and $\boldsymbol{\eta}$ if we use continuous piecewise linear polynomials for all unknown functions. However, in Section 5, our numerical results demonstrate optimal convergence rates. Interestingly, we observe that the weight Δt^2 is crucial for achieving optimal convergence when continuous piecewise linear polynomials are used for all unknowns. On the other hand, the convergence behavior of the a posteriori error estimator $J_{\Delta t^i}^{1/2}$ (4.3) concerning h is numerically tested in the numerical experiments.

5. Numerical implementation

For numerical experiments, we consider the WLS functional in (3.13) for (2.6)–(2.8) and the scaled equation (3.12). The numerical results will be compared with the simulation results obtained using the functional in (3.1) for the standard model equations (2.6)–(2.9). We consider fours WLS functionals: $\mathcal{J}_{\Delta t^2}$ in (3.15), $\mathcal{J}_{\Delta t}$ in (3.16), and $\mathcal{J}_{s\Delta t^2}$ and $\mathcal{J}_{s\Delta t}$, which are defined by \mathcal{J}_s in (3.1) with $(W_1, W_2, W_3, W_4) = (\Delta t^2, 1, \Delta t, 1)$ and $(\Delta t, 1, \Delta t, 1)$, respectively.

5.1. Test problem 1

To investigate the convergence of the proposed WLS methods, we perform numerical experiments using the non-physical example reported in [10]. As shown in [10], we let $\mu = 1$, $K = \mathbf{I}$, $\alpha = 1$ and $c_s = 0$ in (2.6)–(2.8) and (3.12). Consider $\Omega = (0,1)^2$ for the domain of model equations. Let $\phi(x,y) = \sin(2\pi x)\sin(2\pi y)$ and

$$\psi(t) = \frac{1}{64\pi^4 + 4\pi^2} \left(8\pi^2 \sin(2\pi t) - 2\pi \cos(2\pi t) + 2\pi e^{-8\pi^2 t}\right).$$

We can obtain

$$f_s(x, y, t) = \phi(x, y)\sin(2\pi t) + c_s\psi'(t)\phi(x, y),$$

where

$$\psi'(t) = \frac{1}{16\pi^2 + 1} \left(4\pi \cos(2\pi t) + \sin(2\pi t) - 4\pi e^{-8\pi^2 t} \right),$$

and exact solutions

$$p(x,y,t) = \psi(t)\phi(x,y), \quad \mathbf{u}(x,y,t) = -\psi(t)\nabla\phi(x,y), \quad \boldsymbol{\eta}(x,y,t) = -\frac{\psi(t)}{8\pi^2}\nabla\phi(x,y).$$

All exact solutions are enforced on the boundary. In our computations, linear basis functions are considered for all variables. The time step $\Delta t = 0.01$ is chosen for temporal discretization. We discretized Ω by a uniform Union Jack grids sequence with h = 1/8, 1/16, and h = 1/32. Figure 5.1 shows the solution of the WLS with $\mathcal{J}_{\Delta t^2}$ in (3.15) at time t = 0.05 with considerably enlarged deformations and seepage velocity arrows on uniform Union Jack grids with h = 1/32.

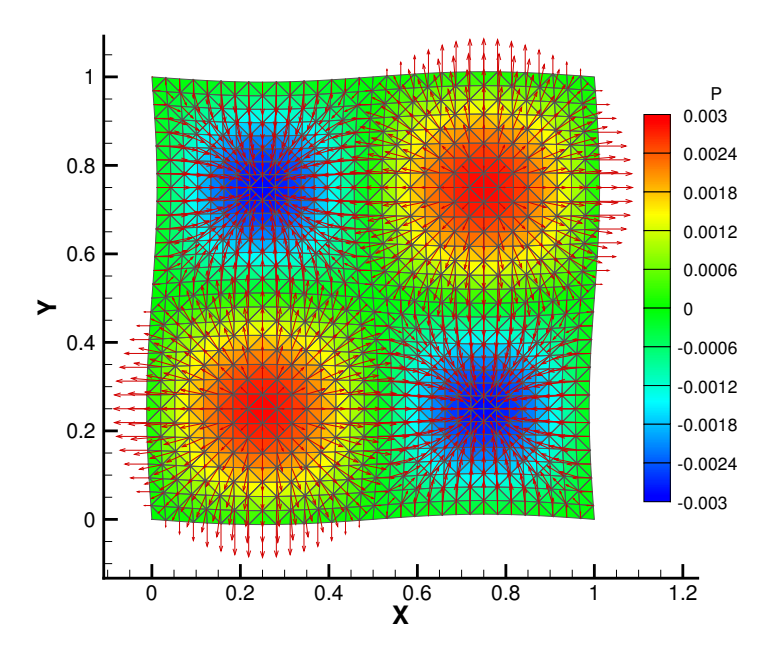


Figure 5.1: The seepage velocity \mathbf{u} (arrows) and the pressure p (contours) on the mesh deformed by fifty times the η size using the WLS with $\mathcal{J}_{\Delta t^2}$ on uniform Union Jack grids.

Next, we present the convergence rates of the WLS solutions for $(\mathbf{u}, p, \boldsymbol{\sigma}, \boldsymbol{\eta})$ using the functionals \mathcal{J} in (3.13) and \mathcal{J}_s in (3.1) with $(W_1, W_2, W_3, W_4) = (\Delta t^2, 1, \Delta t, 1)$, and $(\Delta t, 1, \Delta t, 1)$ at time t = 0.05 in Figures 5.2 and 5.3. Figure 5.2 illustrates convergence rates of O(h) in the norm of $(H^{div}, H^1, H^{div}, H^1)$ for $(\mathbf{u}, p, \boldsymbol{\sigma}, \boldsymbol{\eta})$. Moreover, these results demonstrate optimal convergence of the functional value $J^{1/2}(\mathbf{u}, p, \boldsymbol{\sigma}, \boldsymbol{\eta}; \mathbf{F})$ for $J = \mathcal{J}_{\Delta t^2}$, $\mathcal{J}_{\Delta t}$, $\mathcal{J}_{s\Delta t^2}$, and $\mathcal{J}_{s\Delta t}$ at O(h). These convergence rates are consistent with our analysis in Section 4.

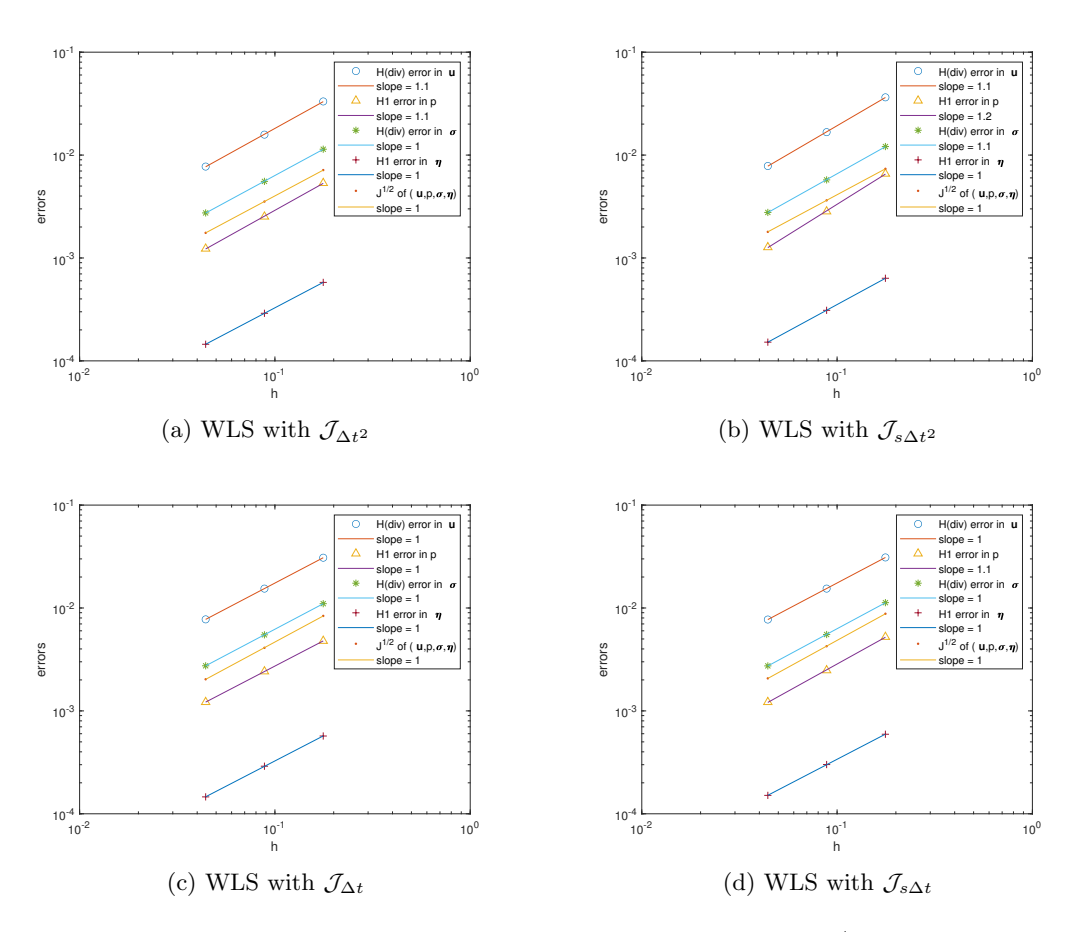


Figure 5.2: H(div) errors of \mathbf{u} , $\boldsymbol{\sigma}$, H^1 errors of p and $\boldsymbol{\eta}$, and $J^{1/2}$ functional value of $(\mathbf{u}, p, \boldsymbol{\sigma}, \boldsymbol{\eta})$ for J as (a) $\mathcal{J}_{\Delta t^2}$, (b) $\mathcal{J}_{s\Delta t^2}$, (c) $\mathcal{J}_{\Delta t}$, and (d) $\mathcal{J}_{s\Delta t}$ at t = 0.05.

In addition, we present the L^2 -norm errors of the WLS solutions in Figure 5.3. As shown in Figure 5.3, the use of the WLS with $\mathcal{J}_{\Delta t^2}$ yields a significant improvement in the convergence of the solution, in particular, \mathbf{u} and $\boldsymbol{\eta}$, compared to the solution obtained using $\mathcal{J}_{\Delta t}$. Also, in Figure 5.3 some improvements are observed when using \mathcal{J} with $(W_1, W_2, W_3, W_4) = (\Delta t^2, 1, \Delta t, 1)$ over \mathcal{J}_s , resulting in the optimal rate $O(h^2)$. This result suggests that the use of the mass conservation weight Δt^2 for \mathcal{J} can improve the

convergence rate of the solution in L^2 -norm to an optimal rate.

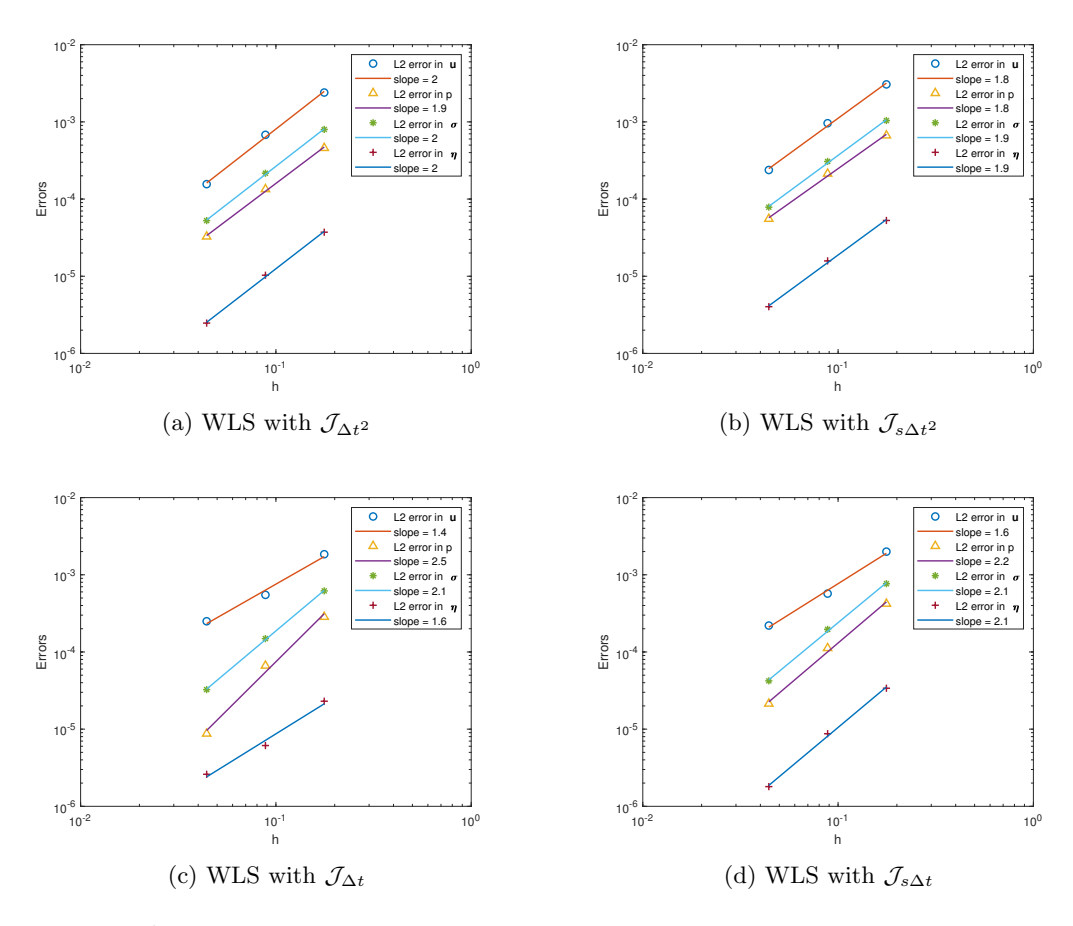


Figure 5.3: L^2 errors of \mathbf{u} , p, $\boldsymbol{\sigma}$, and $\boldsymbol{\eta}$ by WLS methods with (a) $\mathcal{J}_{\Delta t^2}$, (b) $\mathcal{J}_{s\Delta t^2}$, (c) $\mathcal{J}_{\Delta t}$, and (d) $\mathcal{J}_{s\Delta t}$ at t = 0.05.

5.2. Cantilever bracket problem

We consider a cantilever bracket problem presented by Phillips and Wheeler [16], wherein their simulation displays locking in poroelasticity. When the time step, Δt , is small, and if $c_s = 0$ and the permeability is small, the early deformation solution is nearly divergence-free within a short time. This makes it challenging for the numerical method to accurately capture both phenomena, leading to locking. Furthermore, the results in [16] show that continuous bilinear elements cannot approximate a nonconstant, divergence-free deformation. Therefore, alternative spaces must be used for approximating the deformation.

We implement the WLS method using (3.13) to overcome nonphysical oscillations in the pressure variable for a cantilever bracket problem in Figure 5.4. The body force and

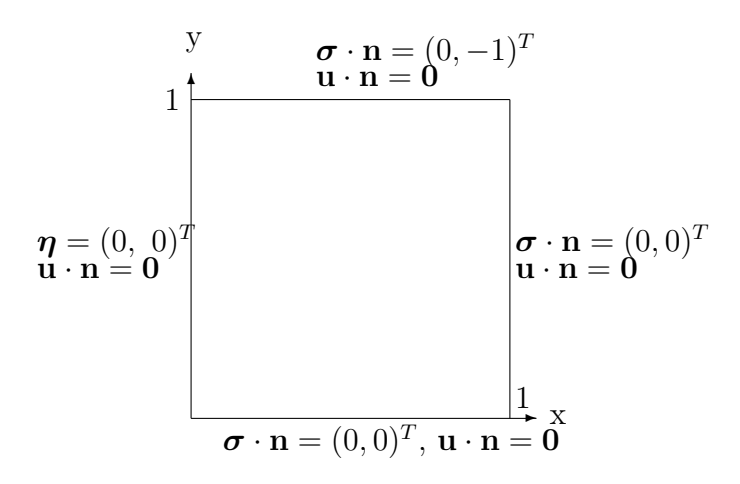


Figure 5.4: Description of the cantilever bracket problem.

the source terms are set to zero, i.e., $\mathbf{f}_b = \mathbf{0}$ and $f_s = 0$. The domain is the unit square $(0,1)^2$. For the flow problem, we impose a no-flow boundary condition along the entire boundary. We assume that the left side edge is fixed for the elasticity problem, assessing a no-displacement boundary condition. Additionally, we impose downward traction at the top side and a traction-free boundary condition at the right and bottom sides. The initial displacement and pressure are assumed to be zero. We conduct numerical simulations based on the physical parameters and boundary conditions used in [18]. Based on [18], the following boundary conditions are considered:

$$\begin{aligned} \mathbf{u}_y &= 0, & \boldsymbol{\sigma}_{yy} &= 0 & \text{on } \{(x,y) \in \partial \Omega : y = 0\}, \\ \mathbf{u}_x &= 0, & \boldsymbol{\sigma}_{xx} &= 0 & \text{on } \{(x,y) \in \partial \Omega : x = 1\}, \\ \mathbf{u}_y &= 0, & \boldsymbol{\sigma}_{yy} &= -1 & \text{on } \{(x,y) \in \partial \Omega : y = 1\}, \\ \mathbf{u}_x &= 0, & \boldsymbol{\eta}_x &= 0, & \boldsymbol{\eta}_y &= 0 & \text{on } \{(x,y) \in \partial \Omega : x = 0\}. \end{aligned}$$

As shown in [7], the displacement vector is no longer divergence-free, so no locking exists at later times. Hence, we set $\Delta t = 0.001$ and use these material parameters: Young's modulus $E = 10^4$, Poisson ration $\nu = 0.45$, percolation coefficient $\kappa = 10^{-7}$, $\alpha = 0.95$, and constrained specific storage coefficient $c_s = 0$.

We consider linear basis functions for all variables and use uniform Union Jack grids in our computations. Figure 5.5 shows the pressure profiles at t = 0.001 using the WLS with $\mathcal{J}_{\Delta t^2}$, $\mathcal{J}_{\Delta t}$, $\mathcal{J}_{s\Delta t^2}$, and $\mathcal{J}_{s\Delta t}$ on various meshes with $h = 2^{-(k+2)}$ for k = 1, 2, 3, 4. We employ the a posteriori error estimator for mesh refinement criteria [14] with the convergence tolerance 10^{-6} ,

$$\frac{\Delta J_{(k)}^{1/2}}{\Delta N_k} := \frac{\left|J_{(k)}^{1/2}(\mathbf{u}, p, \boldsymbol{\sigma}, \boldsymbol{\eta}; \mathbf{F}) - J_{(k-1)}^{1/2}(\mathbf{u}, p, \boldsymbol{\sigma}, \boldsymbol{\eta}; \mathbf{F})\right|}{|N_k - N_{k-1}|},$$

where $N_k = 2h^{-2}$ represents the number of elements at the k-th refinement step. $J_{(k)}^{1/2}(\mathbf{u}, p, \boldsymbol{\sigma}, \boldsymbol{\eta}; \mathbf{F})$ denotes the functional value $J^{1/2}(\mathbf{u}, p, \boldsymbol{\sigma}, \boldsymbol{\eta}; \mathbf{F})$ at the WLS solution by number of elements N_k .

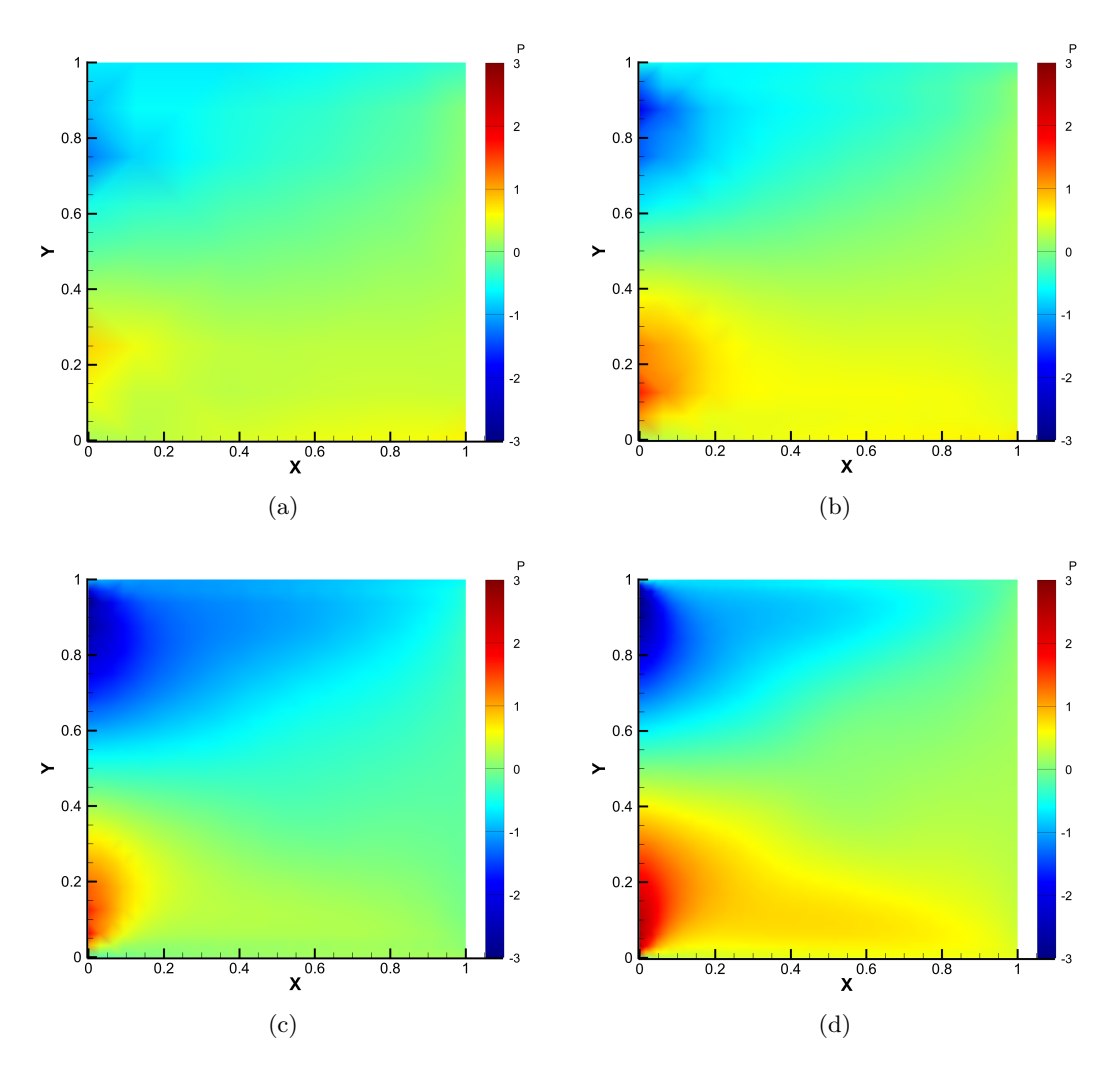


Figure 5.5: Pressure contours at time t = 0.001. Results are produced using the WLS with $\mathcal{J}_{\Delta t^2}$ at (a) h = 1/8, (b) 1/16, (c) 1/32, and (d) 1/64.

Figure 5.6(a) demonstrates mesh convergence for N_k , which is confirmed when $\Delta J_{(k)}^{1/2}/\Delta N_k < 10^{-6}$ for all four functionals $J = \mathcal{J}_{\Delta t^2}$, $\mathcal{J}_{\Delta t}$, $\mathcal{J}_{s\Delta t^2}$, and $\mathcal{J}_{s\Delta t}$. Therefore, we achieve convergent results at k=5 for all cases, and we use the mesh with h=1/128 for the results presented in Figures 5.7. Figure 5.6(b) illustrates the relative error $\delta J^{1/2}$, where $\delta J^{1/2} = (J_{\Delta t^2}^{1/2} - J_{\Delta t}^{1/2})/J_{\Delta t}^{1/2}$ for $J = \mathcal{J}$ and \mathcal{J}_s , at various N_k . It is noteworthy that the errors are negative, indicating that Δt^2 performs better than Δt as a mass conservation weight for both \mathcal{J} and \mathcal{J}_s functionals. Additionally, the difference in performance is more

significant for the functional \mathcal{J} . Figure 5.6(c) shows that \mathcal{J}_s functionals yield the linear convergent rate of $J^{1/2}$, O(h), while the convergence of \mathcal{J} functionals is slightly worse than \mathcal{J}_s . However, the functional values $J^{1/2}$ of \mathcal{J} are much smaller than those of \mathcal{J}_s functionals.

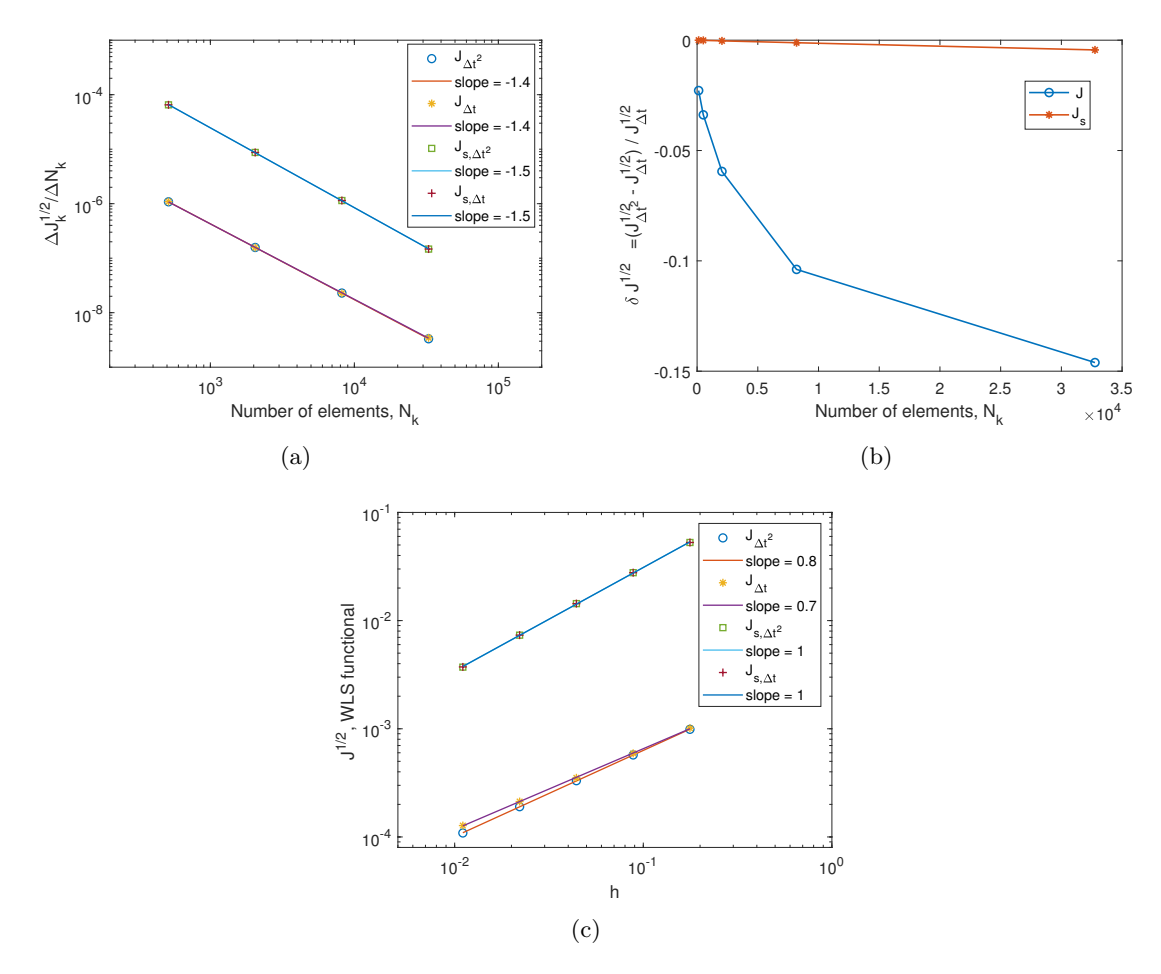


Figure 5.6: (a) Reduction of $\Delta J_{(k)}^{1/2}/\Delta N_k$ versus number of elements N_k . (b) Reduction of $\delta J^{1/2} = (J_{\Delta t^2}^{1/2} - J_{\Delta t}^{1/2})/J_{\Delta t}^{1/2}$ by $J = \mathcal{J}$, \mathcal{J}_s versus number of elements N_k . (c) Convergence of $J^{1/2}$ by $J = \mathcal{J}_{\Delta t^2}$, $\mathcal{J}_{\Delta t}$, $\mathcal{J}_{S\Delta t^2}$, and $\mathcal{J}_{S\Delta t}$.

To demonstrate the effects of different weight choice, we present WLS solutions using \mathcal{J} in (3.13) and \mathcal{J}_s in (3.1) with $(W_1, W_2, W_3, W_4) = (\Delta t^2, 1, \Delta t, 1)$ and $(\Delta t, 1, \Delta t, 1)$. We show pressure profiles for comparing the locking effects of four functional cases in Figure 5.7. Figure 5.7 presents the pressure profiles by the WLS method with $\mathcal{J}_{\Delta t^2}$, $\mathcal{J}_{\Delta t}$, $\mathcal{J}_{s\Delta t^2}$ and $\mathcal{J}_{s\Delta t}$ for t = 0.001. The results show that the WLS method with $\mathcal{J}_{\Delta t^2}$ and $\mathcal{J}_{\Delta t}$ yields smooth pressure profiles, and there are no pressure profiles in all \mathcal{J}_s cases. We obtain a significant pressure profile by the WLS method with $\mathcal{J}_{\Delta t^2}$ over other cases, which

aligns with the results reported in [18]. These results suggest that the locking effect can be effectively resolved by the $\mathcal{J}_{s\Delta t^2}$.

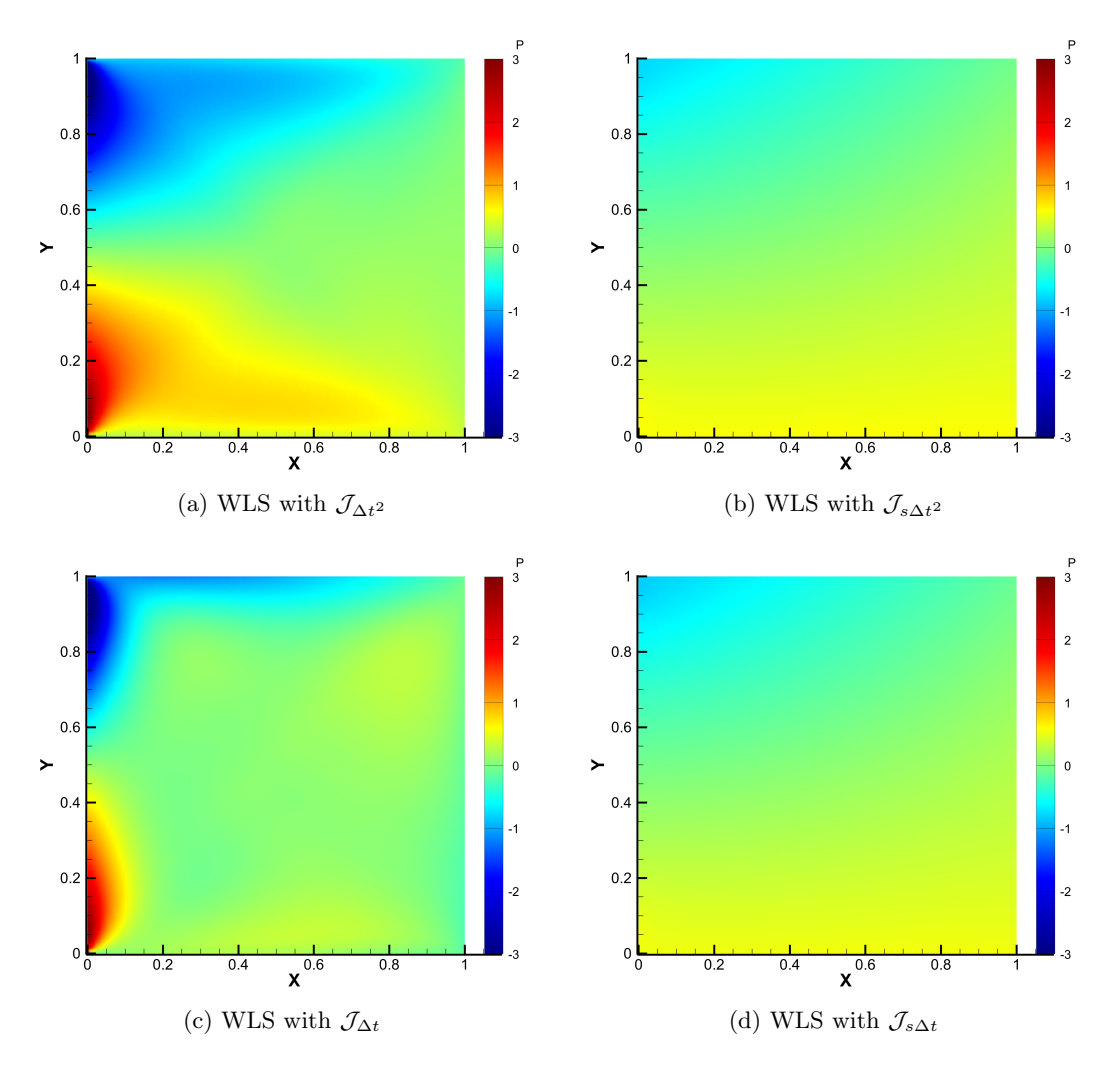


Figure 5.7: Pressure contours at time t = 0.001 on the mesh with h = 1/128. Results are produced using the WLS with (a) $\mathcal{J}_{\Delta t^2}$, (b) $\mathcal{J}_{s\Delta t^2}$, (c) $\mathcal{J}_{\Delta t}$, and (d) $\mathcal{J}_{s\Delta t}$.

6. Conclusion

In this study, we investigated Biot's consolidation problem in rheology using the weighted least squares method. We compared the results obtained using least-squares formulations with different weighting schemes. Our approach utilized lower-order basis functions in all variables. It allowed us to get optimal convergence in all variables in the WLS with the weight $(\Delta t^2, 1, \Delta t, 1)$ for the stress-displacement formulation with $C^{-1/2}$ and $C^{1/2}$. Our results indicate that adjusting the weight of the mass conservation equation in the WLS

method is necessary for obtaining a more accurate and efficient solution. Specifically, using Δt^2 can greatly improve the solutions, resulting in accurate results in the cantilever bracket problem. Additionally, our WLS solutions agreed well with published work, further validating the effectiveness of our approach.

References

- [1] M. A. Biot, General theory of three-dimensional consolidation, J. Appl. Phys. 12 (1941), no. 2, 155–164.
- [2] _____, General solutions of the equations of elasticity and consolidation for a porous material, J. Appl. Mech. 23 (1956), 91–96.
- [3] P. B. Bochev, C. R. Dohrmann and M. D. Gunzburger, Stabilization of low-order mixed finite elements for the Stokes equations, SIAM J. Numer. Anal. 44 (2006), no. 1, 82–101.
- [4] Z. Cai, J. Korsawe and G. Starke, An adaptive least squares mixed finite element method for the stress-displacement formulation of linear elasticity, Numer. Methods Partial Differential Equations 21 (2005), no. 1, 132–148.
- [5] Z. Cai and G. Starke, First-order system least squares for the stress-displacement formulation: Linear elasticity, SIAM J. Numer. Anal. 41 (2003), no. 2, 715–730.
- [6] ______, Least-squares methods for linear elasticity, SIAM J. Numer. Anal. 42 (2004), no. 2, 826–842.
- [7] X. Feng, Z. Ge and Y. Li, Analysis of a multiphysics finite element method for a poroelasticity model, IMA J. Numer. Anal. 38 (2018), no. 1, 330–359.
- [8] B. Gmeiner, U. Rüde, H. Stengel, C. Waluga and B. Wohlmuth, *Performance and scalability of hierarchical hybrid multigrid solvers for Stokes systems*, SIAM J. Sci. Comput. **37** (2015), no. 2, C143–C168.
- [9] C. Helanow and J. Ahlkrona, Stabilized equal low-order finite elements in ice sheet modeling-accuracy and robustness, Comput. Geosci. 22 (2018), no. 4, 951–974.
- [10] G. Kanschat and B. Riviere, A finite element method with strong mass conservation for Biot's linear consolidation model, J. Sci. Comput. 77 (2018), no. 3, 1762–1779.
- [11] J. Korsawe and G. Starke, A least-squares mixed finite element method for Biot's consolidation problem in porous media, SIAM J. Numer. Anal. 43 (2005), no. 1, 318– 339.

- [12] J. Korsawe, G. Starke, W. Wang and O. Kolditz, Finite element analysis of poroelastic consolidation in porous media: Standard and mixed approaches, Comput. Methods Appl. Mech. Engrg. 195 (2006), no. 9-12, 1096-1115.
- [13] H.-C. Lee and T.-F. Chen, A nonlinear weighted least-squares finite element method for Stokes equations, Comput. Math. Appl. **59** (2010), no. 1, 215–224.
- [14] H.-C. Lee and H. Lee, An a posteriori error estimator based on least-squares finite element solutions for viscoelastic fluid flows, Electron. Res. Arch. 29 (2021), no. 4, 2755–2770.
- [15] _____, A weighted least-squares finite element method for Biot's consolidation problem, Int. J. Numer. Anal. Model. 19 (2022), no. 2-3, 386–403.
- [16] P. J. Phillips and M. F. Wheeler, Overcoming the problem of locking in linear elasticity and poroelasticity: An heuristic approach, Comput. Geosci. 13 (2009), no. 1, 5–12.
- [17] M. Tchonkova, J. Peters and S. Sture, A new mixed finite element method for poroelasticity, Internat. J. Numer. Anal. Methods Geomech. **32** (2008), no. 6, 579–606.
- [18] S.-Y. Yi, Convergence analysis of a new mixed finite element method for Biot's consolidation model, Numer. Methods Partial Differential Equations 30 (2014), no. 4, 1189–1210.

Hsueh-Chen Lee

Center for General Education, Wenzao Ursuline University of Languages, 900 Mintsu 1st Road Kaohsiung, Taiwan

E-mail address: 87013@mail.wzu.edu.tw

Hyesuk Lee

School of Mathematical and Statistical Sciences, Clemson University, Clemson, SC 29634-0975, USA

E-mail address: hklee@clemson.edu